Journal of Hazardous Materials 424 (2022) 127434

Contents lists available at ScienceDirect

Journal of Hazardous Materials

journal homepage: www.elsevier.com/locate/jhazmat

Comparative study on bisphenols oxidation via TiO_2 photocatalytic activation of peroxymonosulfate: Effectiveness, mechanism and pathways

Jialin Jia [a], Dongmei Liu [a,*], Qiao Wang [a,d], Huarui Li [a], Jiaxin Ni [a], Fuyi Cui [c], Jiayu Tian [b,*]

[a] State Key Laboratory of Urban Water Resource and Environment, School of Environment, Harbin Institute of Technology, Harbin 150090, China
[b] School of Civil and Transportation Engineering, Hebei University of Technology, Tianjin 300401, China
[c] College of Urban Construction and Environmental Engineering, Chongqing University, Chongqing 400044, China
[d] School of Civil and Transportation Engineering, Guangdong University of Technology, Guangzhou 510006, China

ARTICLE INFO

Editor: Dr. B. Lee

Keywords:
Peroxymonosulfate activation
TiO_2 nano-tubes arrays
Bisphenol F
Bisphenol AF
Bisphenol S

ABSTRACT

In this work, degradation of bisphenol F (BPF), bisphenol AF (BPAF) and bisphenol S (BPS) by peroxymonosulfate (PMS) with TiO_2 nano-tubes arrays (TiO_2NTAs) under simulated sunlight irradiation was investigated and compared for the first time. All three bisphenols exhibited appreciable degradation following the order of BPS < BPAF < BPF, and acidic conditions were more conducive to their degradation. The $SO_4^{\bullet-}$, ·OH, h^+ and $^{\bullet}O_2^-$ were all identified in three bisphenols degradation processes. Among these, $SO_4^{\bullet-}$ and $^{\bullet}O_2^-$ were proven to play a dominant role in BPF oxidation process, but $SO_4^{\bullet-}$ and h^+ were confirmed as the main reactive species for BPAF and BPS removal. Owing to the different reactive species worked in different bisphenols degradation processes, the influences of inorganic anions on three bisphenols degradation were also different. By analyzing the oxidation intermediates of the three bisphenols, it was found that there were some common degradation pathways including bond-cleavage and hydroxylation of the benzene ring shared by three bisphenols. Besides, some specific degradation pathways were also identified, for example, the self-coupling was found in BPF and BPS degradation process, while the benzene ring splitting was occurred only in BPAF transformation process

1. Introduction

Bisphenols are extensively employed as additives to enhance transparency and mechanical properties of plastic products (Rochester and Bolden, 2015). Among which, as one of the most commonly consumed bisphenols, bisphenol A (BPA) has been prohibited or controlled by many countries since it was a bio-accumulative endocrine disruptors and could jeopardize the metabolic and reproductive system of mammals (Newbold et al., 2009; Richter et al., 2007). For this reason, some BPA-substitutes began to be produced and applied, and the detection frequency of these substitutes in environmental samples (such as surface water, river sediment, sewage sludge and indoor dust) and human samples (serum, milk and urine) are rising in recent years (Zhu et al., 2018; Deceuninck et al., 2015). For instance, Yamazaki et al. Yamazaki et al. (2015) reported that the amount of bisphenol F (BPF) was greater than BPA in sea water and surface water samples in Japan, Korea and China in the years of 2013–2014. Song et al. Song et al. (2012) reported that the concentration of bisphenol AF (BPAF) in soils and sediments around a manufacturing plant could reach to 331 and 2.0×10^3 ng/g dry weight (dw), respectively. Liao et al. Liao et al. (2012) reported that the bisphenol S (BPS) content in sediments of Japan, Korea, and China could reach 1.97×10^3 ng/g dw. Since their structure is similar to that of BPA (the three bisphenols chemical formular were shown in Fig. 1), BPF, BPAF and BPS could also display endocrine disrupting effects based on recent studies (Hashimoto and Nakamura, 2000; Fic et al., 2013; Moreman et al., 2017). Once they are released or migrated into the aquatic environment, it may arouse new water ecological problems. Thus, removing these bisphenols from water bodies is very important for protecting human and aquatic organisms.

Many oxidation methods including manganese dioxide (Li et al., 2018), chlorine (Gao et al., 2018), persulfate (Wang et al., 2019) and ferrate oxidation (Yang et al., 2020) have been employed to remove the bisphenols in water environment. Among which, PMS-based advanced oxidation processes (AOPs) have received tremendous attention due to the good chemical stability, commercially available features, and formation of highly active species (such as $SO_4^{\bullet-}$ and ·OH) (Li et al., 2018). However, PMS without activation exhibited low reactivity for organic pollutants decomposition (Wacławek et al., 2017). Thereafter, various

* Corresponding authors.
E-mail addresses: ldm819@126.com (D. Liu), tjy800112@163.com (J. Tian).

https://doi.org/10.1016/j.jhazmat.2021.127434
Received 17 June 2021; Received in revised form 7 September 2021; Accepted 3 October 2021
Available online 6 October 2021

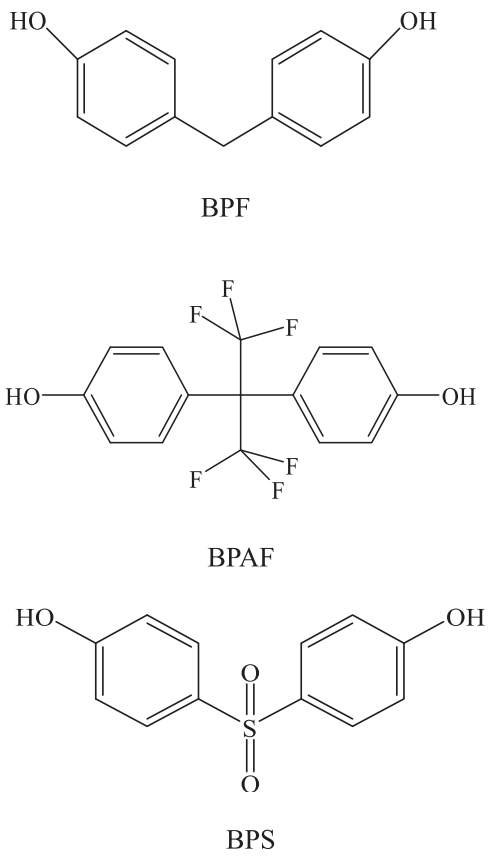

Fig. 1. Chemical formula of BPF, BPAF and BPS.

methods such as ultrasound (Liu et al., 2017), heat (Tan et al., 2015), ultraviolet light (Ao and Liu, 2017), electrochemistry method (Chen and Huang, 2015), alkaline (Qi et al., 2016), quinone (Oh et al., 2018), phenol (Zhang et al., 2016), metal oxides/transition metals (Anipsitakis and Dionysiou, 2004; Nie et al., 2015), carbon catalysts (Chen et al., 2018) and semiconductors (Gao et al., 2017) have been developed for activating PMS to generate reactive species for the degradation of organic pollutants. Nevertheless, most of above methods usually need large amounts of energy or chemical input (for preparing catalyst and/or inducing PMS activation), and may exert secondary contamination problems (leaking metal ions or powder catalysts), which limited their large-scale application in practical water remediation. Developing a relatively economic and eco-friendly method for PMS activation is still urgently needed.

Semiconductors photocatalysis is an ideal technology for water remediation owing to the use of renewable solar energy (Wang et al., 2018). Among various semiconductors, TiO_2 is deemed as the most suitable photocatalyst for extensive environmental applications due to high chemical stability, non-toxic and cheapness, which was also used in combination with other AOPs (Andersson et al., 2002). Combining TiO_2 photocatalysis with PMS oxidation has been proved an effective approach to degrade organic pollutants. For example, Chen et al. Chen et al. (2012) reported that the Acid Orange 7 (AO7) was effectively removed by TiO_2/PMS system under visible light irradiation. Xu et al. Xu et al. (2020) reported that 100% of PFOA could be removed within 9 h by TiO_2/PMS system under visible light, while in real wastewater, 100% of PFOA could be degraded in TiO_2/PMS system within 2 h under UV light. Khan et al. Khan et al. (2017) demonstrated that an effective removal of lindane could be achieved by sulfur doped TiO_2 (S-TiO_2)/PMS under light irradiation, where the degradation rate of lindane could reach to 68.2% and 99.9% after 6 h of visible light and simulated sunlight irradiation, respectively. Inspired by these studies, the efficient removal of bisphenols in TiO_2/PMS system under light irradiation may also be feasible. However, so far, the degradation behaviors of bisphenols in the TiO_2/PMS system under simulated sunlight irradiation still blurred and unexplored.

Hence, in this work, three commonly used BPA-substitutes: bisphenol F (BPF), bisphenol AF (BPAF) and bisphenol S (BPS) were selected as the target pollutants and their degradation behaviors were comparatively investigated in the TiO_2/PMS system under simulated sunlight irradiation. To avoid the problem of difficult separation and recovery of powder catalyst, TiO_2 nano-tubes arrays (TiO_2NTAs), which in situ grew on Ti plate by anodization strategy were employed as the photocatalyst and activator of PMS. The degradation performances of three bisphenols were assessed, and the underlying mechanism, including reactive species, oxidation intermediates and degradation pathways were also studied and discussed systematically.

2. Experimental

2.1. Materials

BPF, BPAF and BPS were purchased from Sigma Aldrich Co. Ltd., USA. Titanium plates (0.5 mm thickness, 99.8% purity) were obtained from Dongguan Fu Tai Metal Materials Co., Ltd. Peroxymonosulfate (PMS, $\geq$ 47% $KHSO_5$), methanol (MeOH), *tert*-butanol (TBA), 5,5-dimethyl-1-pyrroline-N-oxide (DMPO), humic acid (HA) were all purchased from Aladdin Chemistry Co., Ltd (Shanghai, China). All the other chemicals were reagent grade and were obtained from Sinopharm Chemical Reagent Co., Ltd (Shanghai, China). Deionized (DI) water was employed throughout the experiments.

2.2. Preparation of TiO_2NTAs

TiO_2 nano-tube arrays (TiO_2NTAs) were fabricated on Ti plates by conducting an anodization strategy. Before anodization, Ti plates were pre-processed based on the earlier report (Li et al., 2016). The anodization process was conducted in a glycerol aqueous solution (glycerol: water = 60%:40% in volume) containing 0.5 wt% ammonium fluoride (NH_4F), in which the Ti plate and Pt foil were set as the anode and cathode, respectively. The two electrodes were placed face to face with a distance of 2 cm. An applied potential of 20 V was conducted for 2 h under room temperature. Subsequently, the as-anodized TiO_2NTAs samples were rinsed with deionized water for several times before drying at 70 °C for 4 h. Lastly, TiO_2NTAs of anatase phase was obtained by calcining at 500 °C for 2 h with a heating rate of 3 °C/min.

2.3. Characterization

The morphology of TiO_2NTAs was observed by using a field emission scanning electron microscope (FE-SEM, Zeiss SUPRA 55 SAPPHIRE). The crystal structure of TiO_2NTAs was recorded with a Bruker D8 X-ray diffractometer with Cu Ka radiation ($\lambda = 0.15418$ nm). The optical property was investigated by UV–vis diffuse reflectance spectra (DRS) (Shimadzu, UV2550). The reactive species were identified by Electron spin resonance (ESR) spectroscopy (Bruker A300 spectrometer, Germany).

2.4. Experimental procedures

The degradation experiments were carried out in a 100 mL beaker containing 50 mL aqueous solution of bisphenols (10 mg/L) under magnetic stirring. A 300 W xenon lamp (Beijing, NBeT) with an AM 1.5 G filter (Beijing, NBeT) was used as the simulated sunlight source. The distance between the light and solution interface was set to 10 cm, and the light intensity irradiated on the surface of reaction solution was 100 mW cm^{-2} (one-sun intensity). Before irradiation, the as-prepared TiO_2NTAs was fixed in the beaker, and the reaction area of the

photocatalyst was set at 1 × 2 cm^2. Afterwards, PMS was introduced into the beaker to trigger the reaction with the xenon lamp switched on. The temperature of the reaction system was kept at 25 ± 2 °C by continuous circulation of cooling water (the reaction equipment was shown in Fig. S1). At desired time intervals, the reaction solution was withdrawn and filtered through 0.22 μm PTFE membranes, and then 1 mL of filtrate was quickly injected into a brown vial containing excess MeOH to stop the reaction. The samples were stored at 4 °C in dark before analysis. All experiments were performed in duplicates or triplicates, and the average values with the standard deviations were recorded.

2.5. Analytical methods

The concentrations of BPF, BPAF and BPS were determined by a HITACHI HPLC system with a Symmetry C18 column (5 μm particle size, 4.6 × 150 mm) and a HITACHI 5430 diode array detector at UV wavelengths of 230 nm, 230 nm and 260 nm, respectively. The mobile phase was composed of methanol and 0.1% acetic acid at a ratio of 60:40 (v/v), 25:75 (v/v) and 50:50 (v/v) for BPF, BPAF and BPS, respectively, and the flow rate was 1 mL/min. The total organic carbon (TOC) was determined by a Multi N/C 3100 TOC analyzer.

The oxidation products of three bisphenols were identified by HPLC/ESI-MS/MS, which was carried out on a SCIEX QTrap 5500 coupled with an Agilent 1260 HPLC. HPLC separation was conducted on a C18 column (2.5 μm particle size, 3.0 × 100 mm) and 20 μL sample was injected. Gradient mobile phase consists of water (phase A) and acetonitrile (phase B) with a flow rate of 0.2 mL/min. Firstly, the mobile phase with 5% B was maintained for 5 min, after that, the phase B was linearly increased from 5% to 95% B in the next 10 min and kept for 40 min, and then was reverted back to 5% B for 10 min to reach equilibration again. Electrospray ionization (ESI-) with negative mode was used to determine the mass spectra from 40 to 1000 *m/z*. The ion spray floating voltage was 4500 V, the source temperature was 500 °C, the curtain gas and nebulizer gas was set as 35 psi and 50 psi, respectively. The declustering potential (DP) was − 100 V and the collision energy (CE) was − 30–45 V.

3. Results and discussion

3.1. Characterization of the TiO_2NTAs

Fig. 2a displays the top-view FE-SEM image of the as-prepared TiO_2NTAs. As can be seen, the highly ordered TiO_2 nanotubes arrays were grew vertically on the Ti plate, the average inner diameter and the wall thickness of TiO_2 nanotubes were 100 nm and 20 nm, respectively. Fig. 2b presents the XRD patterns of TiO_2NTAs and virgin Ti plate. According to the characteristic peaks of the TiO_2 anatase phase (JCPDS NO. 21-1272) and the Ti metal phase (JCPDS NO. 44-1294), TiO_2NTAs crystallite phase was identified in the XRD patterns. From Fig. 2b it can be seen that in addition to the titanium matrix diffraction peaks, TiO_2NTAs also display two peaks at 25.3° and 48.1°, which could be ascribed to the anatase phase of TiO_2, implying that TiO_2 nanotubes array of anatase phase were successfully synthesized. The optical property of TiO_2NTAs was studied by UV–vis DRS spectra (Fig. 2c). It can be clearly seen that TiO_2NTAs mainly absorbed the ultraviolet light absorption (λ < 400 nm), corresponding to the inherent band gap of TiO_2. Besides, it also exhibited visible light absorption from 400 to 800 nm, which might be ascribed to some colored centers/the trapped charge carriers, and the incident light absorption of TiO_2 based on previous reports (Li et al., 2016, 2021).

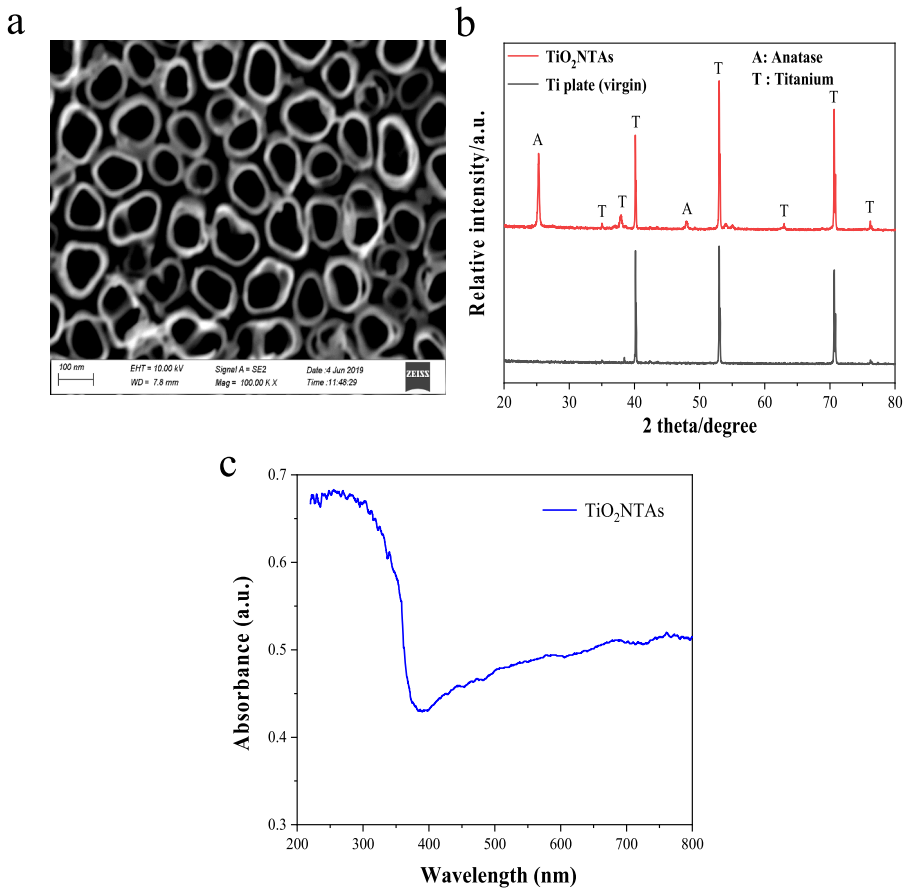

Fig. 2. (a) SEM image, (b) X-ray diffraction (XRD) pattern and (c) UV–vis diffuse reflection spectra of TiO_2NTAs.

3.2. Removal of Bisphenols by TiO_2NTAs/PMS/VL system

The degradation efficiency of three bisphenols by different reaction systems was investigated and compared at neutral pH condition (pH 7.0 ± 0.2). As shown in Fig. 3, bisphenols degradation in the absence of TiO_2NTAs and PMS (blank group) was negligible, which ruled out the possibility of self-degradation induced by SL photolysis. When without light irradiation, essentially no bisphenols removal were observed in the TiO_2NTAs group within 60 min, indicating the fairly weak affinity between the bisphenols and TiO_2NTAs. The addition of PMS resulted in a slight degradation of three bisphenols (< 10%), which could be ascribed to the direct oxidation of PMS. The similar result was also obtained in the TiO_2NTAs/PMS/Dark system, suggesting that TiO_2NTAs could hardly activate PMS without light irradiation. For the TiO_2NTAs/SL group, the marginal degradation of the three bisphenols could be attributed to the photocatalysis induced by TiO_2NTAs itself. As for PMS/SL group, the removal of bisphenols might be ascribed to the PMS activation by a small part of ultraviolet in the SL. Surprisingly, the degradation efficiencies of three bisphenols were substantially improved in the TiO_2NTAs/PMS/SL system, with the removal efficiencies reaching to 90.4%, 84.7% and 70.5% for BPF, BPAF and BPS, respectively, indicating that TiO_2NTAs could effectively activate PMS under SL irradiation. In addition, kinetic analysis displayed that degradation of three bisphenols followed the first-order kinetics and the rate constants of the TiO_2NTAs/PMS/SL system were much higher compared to other reaction systems (Fig. S2 and Table S1).

As can be seen in Table S1, the kinetic constants (k) of three bisphenols followed the order of BPF > BPAF > BPS. As one of the dissociated phenols, BPF is more reactive to electrophilic agents (oxidants) than that of non-dissociated phenols because of its higher electron density (Stone, 1987). For BPAF, F atoms are electron-withdrawing groups and are inactive with PMS, thus leading to a low reactivity of BPAF towards oxidants. Besides, the lower reactivity of BPS towards PMS than BPAF may ascribe to the stronger electron withdrawing effect of SO_2 group than that of F atoms on the aromatic ring. The similar effects of substituent on reactivity of the bisphenols were also found during the permanganate and chlorine oxidation processes (Gao et al., 2018; Jiang et al., 2010).

The mineralization ability of TiO_2NTAs/PMS/SL system was explored since the total organic carbon (TOC) is also a vital index in water treatment. In Fig. S3, after 120 min reaction, the TOC removal efficiencies of three bisphenols by TiO_2NTAs/PMS/SL system were 61.6% (BPF), 48.4% (BPAF) and 42.0% (BPS), respectively, while, three bisphenols were hardly mineralized in the PMS/SL and TiO_2NTAs/SL systems (all below 5%). This indicated that TiO_2NTAs/PMS/SL system exhibited high mineralization capacity, and can be employed as a candidate for water treatment.

3.3. Stability of TiO_2NTAs

Additionally, the stability of the prepared TiO_2NTAs was evaluated and a series of cyclic degradation experiments were conducted. As shown in Fig. S4, the removal efficiency of three bisphenols exhibited a slight reduction (all below 10%) after 30 tests. This might be due to that the degradation intermediates of bisphenols adsorbed on the TiO_2NTAs surface, which impaired the photocatalytic property of TiO_2NTAs and the corresponding PMS activation efficiency. To prove our conjecture, the FT-IR characterization of the used TiO_2NTAs was recorded. As shown in Fig. S5, after 30 cycles, besides the characteristic peak of Ti–O–Ti stretch at 580 cm^{-1}, there was another peak appeared at about 750–900 cm^{-1}, this peak can be ascribed to the characteristic peak of C–H bond of organics (Kuehn et al., 1982; Vassallo et al., 1991), which was the direct evidence that the degradation products of bisphenols adsorbed on the surface of TiO_2NTAs. In addition, the –OH peak at around 3400 cm^{-1} disappeared after 30 cycles in the used TiO_2NTAs, this might be due to the fact that the degradation products adhered on the surface of TiO_2NTAs and covered the –OH peak. Nevertheless, after ultrasonic treatment of the used TiO_2NTAs for 30 s in the dilute acid solution, the performance of TiO_2NTAs/PMS/SL system could recover to the initial level even after 60 cycles.

The stability of TiO_2NTAs was further studied by SEM and XRD characterizations after 30 cycles. As shown in Fig. S6a and b, the morphology of TiO_2NTAs almost unchanged after 30 cycles, and Fig. S6c shows that the anatase phase characteristic peaks of TiO_2 at 25.3° and 48.1° were still well crystalline after 30 cycles. The above results manifested that TiO_2NTAs owned a fairly excellent stability and could be employed as a prospective material in PMS activation for organic pollutants removal in practice.

3.4. Effect of water matrices on bisphenols degradation

3.4.1. pH

The pH value has a great impact on the removal of organic pollutants during oxidation processes since it can influence the charge of substrate and the surface charge properties of the catalyst. Therefore, influence of initial pH on TiO_2NTAs/PMS/SL system for bisphenols degradation was investigated. As shown in Fig. 4, with the initial pH increasing from 3.0 to 9.0, the removal efficiencies of all three bisphenols decreased. This phenomenon can be explained by that PMS exists as anion in a wide pH range (pKa1 = 0.4, pKa2 = 9.3) (Elias et al., 1994). While, the surface of

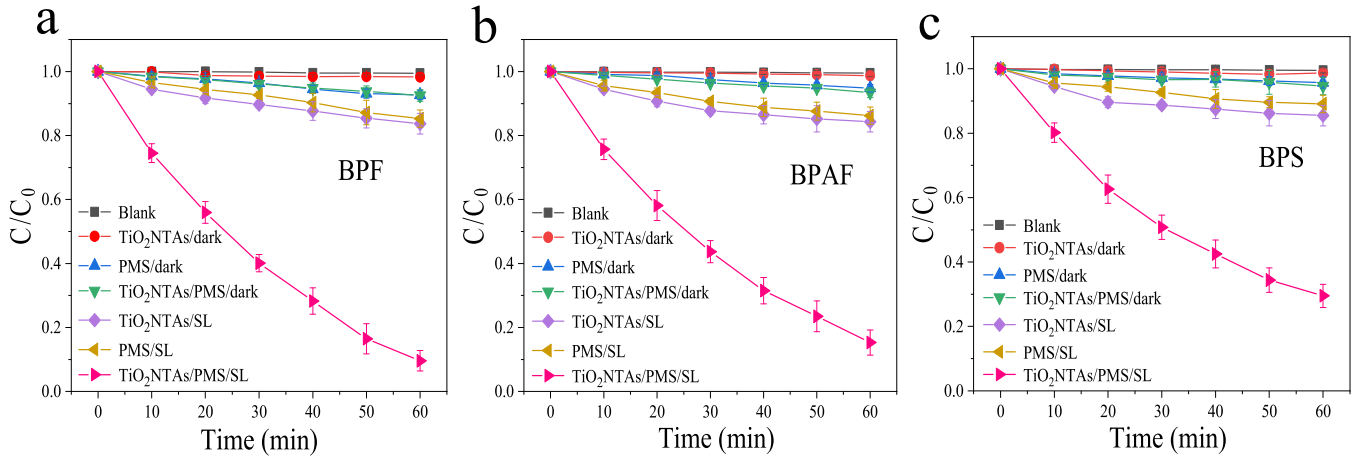

Fig. 3. Bisphenols degradation in different systems: (a) BPF, (b) BPAF, (c) BPS. Reaction conditions: [PMS] = 0.5 mM, [BPF] = [BPAF] = [BPS] = 10 mg/L, [initial pH] = 7, T = 25 °C.

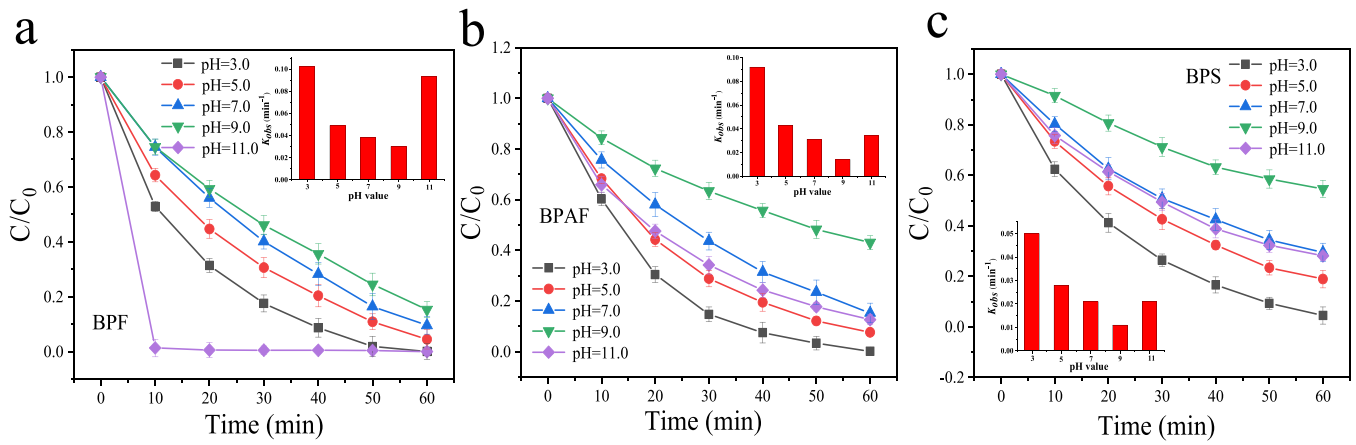

Fig. 4. Effect of pH on (a) BPF, (b) BPAF and (c) BPS degradation in the TiO_2NTAs/PMS/SL system. Reaction conditions: [PMS] = 0.5 mM, [BPF] = [BPAF] = [BPS] = 10 mg/L, [initial pH] = 3–11, T = 25 °C.

TiO_2 is positively and negatively charged under acidic and alkaline conditions, respectively (the PZC of TiO_2 is 6.3) (Halmann, 1996). Because of the electrostatic attraction, there were more probabilities for PMS to react with TiO_2 under acidic conditions, which leaded to the formation of more reactive species. On the contrary, due to the electrostatic repulsion between PMS and TiO_2 under alkaline conditions, PMS has less opportunities to contact with TiO_2, resulting in the less production of reactive species. As a result, degradation of three bisphenols was hindered. However, with the initial pH further increased to 11.0, the removal efficiencies of three bisphenols were all promoted. This might be ascribed to the alkali activating PMS, where the negatively charged -OH was prefer to donate electron compared to H_2O molecules (Duan et al., 2016). Besides, the reaction between the photo-induced holes (h^+) and OH^- is also highly correlated with the solution pH (Zhang et al., 2020). As shown in Eq. (1), the dissolved O_2 could react with photo-induced electron (e^-) to generate $^{\bullet}O_2^-$, then the produced $^{\bullet}O_2^-$ would react with the H^+ in the solution with the presence of another e^- to generate H_2O_2 (Eq. (2)), which would turn into ·OH via Eqs. (3) and (4) (Cui et al., 2012).

$$O_2 + e^- \rightarrow {}^{\bullet}O_2^- \quad (1)$$

$$^{\bullet}O_2^- + 2H^+ + e^- \rightarrow H_2O_2 \quad (2)$$

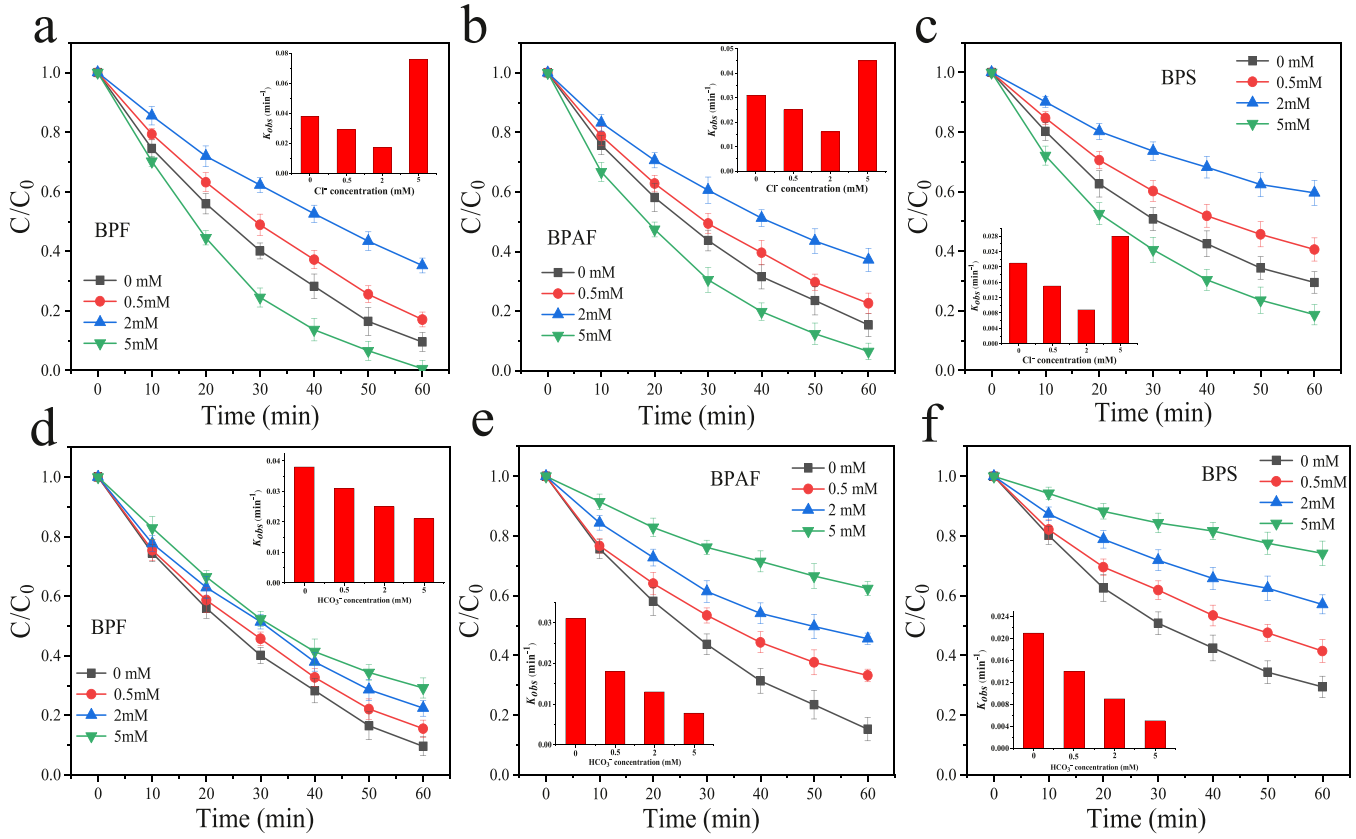

Fig. 5. Effect of Cl^- (a, b, c) and HCO_3^- (d, e, f) on BPF, BPAF and BPS degradation in the TiO_2NTAs/PMS/SL system. Reaction conditions: [PMS] = 0.5 mM, [BPF] = [BPAF] = [BPS] = 10 mg/L, [Cl^-] = [HCO_3^-] = 0–5 mM, [initial pH] = 7, T = 25 ℃.

$$H_2O_2 + e^- \rightarrow \cdot OH + OH^- \quad (3)$$

$$h^+ + OH^- \rightarrow \cdot OH \quad (4)$$

Obviously, H^+ concentration in the system can affect the generation of oxygen species during the degradation process. Noted that at pH 11, BPF was almost completely removed within 10 min (Fig. 4a), which was much higher than that of BPAF (87.3% at 60 min) (Fig. 4b) and BPS (71.9% at 60 min) (Fig. 4c). This is because that as the pH value increased, concentration of H^+ in the system decreased accordingly, thus resulting in the less consumption of $^{\bullet}O_2^-$ in the system, which was confirmed to be one of the primary reactive species for BPF degradation (Section 3.6.1). However, for BPAF and BPS, h^+ has been demonstrated as one of the dominant reactive species (Section 3.6.1), and due to the electro-positivity, the oxidizing capacity of h^+ would decrease with the solution pH value increased (Akpan and Hameed, 2009; Shi et al., 2013), thus the removal efficiencies of BPAF and BPS were lower than that of BPF at pH 11.

3.4.2. Cl^-

As one of the most common inorganic anions in real water bodies, the influences of Cl^- on the degradation of three bisphenols in the TiO_2NTAs/PMS/SL system were explored. As displayed in Fig. 5a-c, Cl^- exhibited the dual effects on three bisphenols degradation. With the Cl^- concentration increased from 0 to 2 mM, removal efficiencies of three bisphenols decreased. However, as the Cl^- concentration further increased to 5 mM, the degradation of three bisphenols was promoted. Similar phenomenon in the PMS-based AOPs process was also found by Zhou et al. (2015) and Wang et al. (2011). The suppressive effect of Cl^- at low concentration might be attributed to the reaction between Cl^- and $SO_4^{\bullet-}$ (one of the main reactive species for three bisphenols degradation as discussed in Section 3.6.1), which resulting in the formation of low-reactive chlorine radicals (Eq. (5)) (Yuan et al., 2011). Consequently, a portion of generated $SO_4^{\bullet-}$ was consumed by Cl^-, reducing the bisphenols degradation. On the other hand, the promotion effects of Cl^- at high concentrations might be due to the fact that the excess Cl^- would react with HSO_5^- to form Cl_2 and HOCl (Eqs. (6)–(7)), which can also oxidize bisphenols (Oh et al., 2016).

$$SO_4^{\bullet-} + Cl^- \rightarrow SO_4^{2-} + Cl\cdot \quad (5)$$

$$2Cl^- + HSO_5^- + H^+ \rightarrow SO_4^{2-} + Cl_2 + H_2O \quad (6)$$

$$Cl^- + HSO_5^- \rightarrow SO_4^{2-} + HOCl \quad (7)$$

3.4.3. HCO_3^-

Fig. 5d-f depict the influence of HCO_3^- on the three bisphenols degradation in the TiO_2NTAs/PMS/SL system. It can be seen that the degradation of all three bisphenols was inhibited after adding HCO_3^- into the system. This could be attributed to that HCO_3^- was an effective scavenger of ·OH and $SO_4^{\bullet-}$ as illustrated in (Eqs. (8)–(9)), and the oxidation ability of the generated $CO_3^{\bullet-}$ was significantly weaker than that of $SO_4^{\bullet-}$ and ·OH (Ghauch and Tuqan, 2012). In addition, the degradation of BPF was less influenced by the HCO_3^- compared with BPAF and BPS. As an alkaline substance, addition of $NaHCO_3$ would raise the pH value of reaction solution. As discussed in Section 3.6.1, h^+ was one of the primary reactive species responsible for BPAF and BPS degradation. The oxidizing ability of h^+ would recede with the increase of pH, thus resulting in a rapid reduction in degradation efficiency of BPAF and BPS. As for BPF, $^{\bullet}O_2^-$ was one of the crucial reactive species for BPF degradation (Section 3.6.1). Although $SO_4^{\bullet-}$ could be quenched by HCO_3^-, increase of the solution pH would reduce the consumption of $^{\bullet}O_2^-$, hence adding HCO_3^- showed slightly inhibition on the BPF removal.

$$SO_4^{\bullet-} + HCO_3^- \rightarrow SO_4^{2-} + HCO_3^{\bullet} \quad (8)$$

$$\cdot OH + HCO_3^- \rightarrow CO_3^{\bullet-} + H_2O \quad (9)$$

3.4.4. HA

As an important component of natural organic matter, HA are widely distributed in surface water, and have complicated effects on oxidation process due to the complex molecular structures. Thus, effects of HA on three bisphenols degradation in the TiO_2NTAs/PMS/SL system were investigated. As depicted in Fig. 6, the degradation rates of three bisphenols were all promoted with increase of HA concentration from 0 to 2 mg/L. Generally, as a radical scavenger, HA could consume $SO_4^{\bullet-}$ and ·OH generated in the system, meanwhile, HA could also be adsorbed onto the surface of catalyst and occupy reactive sites to retard the reaction (Hu et al., 2017). Interestingly, Cho and Choi (2002) found that as a photosensitizer, HA could be excited by visible light and eject electrons to the CB of TiO_2, which then degraded the pollutants via a series of electron transfer processes. In this study, the promotion effect might be also ascribed to this reason. As a photosensitizer, the excited HA by SL could inject electrons to the CB of TiO_2, and then PMS as the electron acceptor would combine with the electrons to generate the corresponding reactive species. However, with the HA dose further increased to 5 mg/L, degradation of bisphenols was inhibited. This might be due to the fact that: (i) the excess HA could occupy the reactive sites of TiO_2NTAs to reduce the generation of reactive species, (ii) HA would compete with TiO_2NTAs for photons, resulting in the less formation of reactive species in the system, and the overmuch HA might act as light screens, which would decrease the light reception of the system.

3.5. Performance in actual water bodies

To explore the practical applicability of the TiO_2NTAs/PMS/SL system, ground water and tap water were employed to investigate the performance of TiO_2NTAs/PMS/VL system. The water quality parameters of the two water bodies were shown in Table S2. As shown in Fig. S7, removal efficiencies of three bisphenols were greatly improved in two water bodies, especially in tap water. For example, BPF could be completely removed within 20 min in tap water, which was in stark contrast to the degradation rate of 90.4% within 60 min in deionized water. Besides, all three bisphenols could be completely removed within 60 min in ground water and tap water. Based on the characteristic of the two water bodies (Table S2) and the discussion of Section 3.4, it can be speculated that the organic carbon and/or Cl^- might promote the three bisphenols degradation in the two real water bodies (Jia et al., 2020). The high bisphenols removal efficiency in actual water bodies further verified the practicability of the TiO_2NTAs/PMS/SL system.

3.6. Proposed activation mechanism

3.6.1. Active species generated in photodegradation processes

In order to determine the active species generated in the TiO_2NTAs/PMS/SL system, the ESR measurements using DMPO as the radical spin trapping agent were conducted. As shown in Fig. 7a and b, under dark condition, there was no characteristic signal of any kind of active species appeared. Nevertheless, with the xenon lamp was switched on, the characteristic signals of DMPO-$SO_4^{\bullet-}$ adduct and DMPO-·OH adduct with the peak intensity ratio of 1:2:2:1 were clearly detected (Fig. 7a) (Wang et al., 2015). In addition, the characteristic peaks of the DMPO-$^{\bullet}O_2^-$ adduct with an intensity ration of 1:1:1:1 were also observed (Fig. 7b) (Zhang et al., 2016). This manifested that $SO_4^{\bullet-}$, ·OH and $^{\bullet}O_2^-$ were all generated in the TiO_2NTAs/PMS/SL system. Noted, the previous studies had suggested that the singlet oxygen ($^1O_2$) might also involve in the PMS oxidation process (Wang et al., 2019; Jia et al., 2020), however, when the TEMP was employed as the spin trapping agent, no typical 1:1:1 triplet characteristic peaks of TEMP-$^1O_2$ were

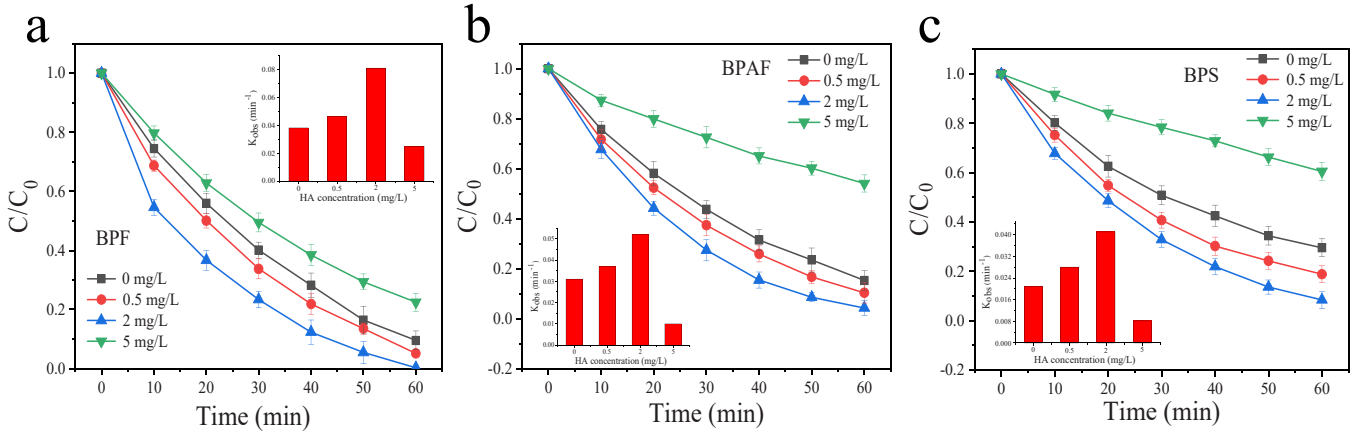

Fig. 6. Effect of HA on (a) BPF, (b) BPAF and (c) BPS degradation in the TiO_2NTAs/PMS/SL system. Reaction conditions: [PMS] = 0.5 mM, [BPF] = [BPAF] = [BPS] = 10 mg/L, [HA] = 0–5 mg/L, [initial pH] = 7, T = 25 ℃.

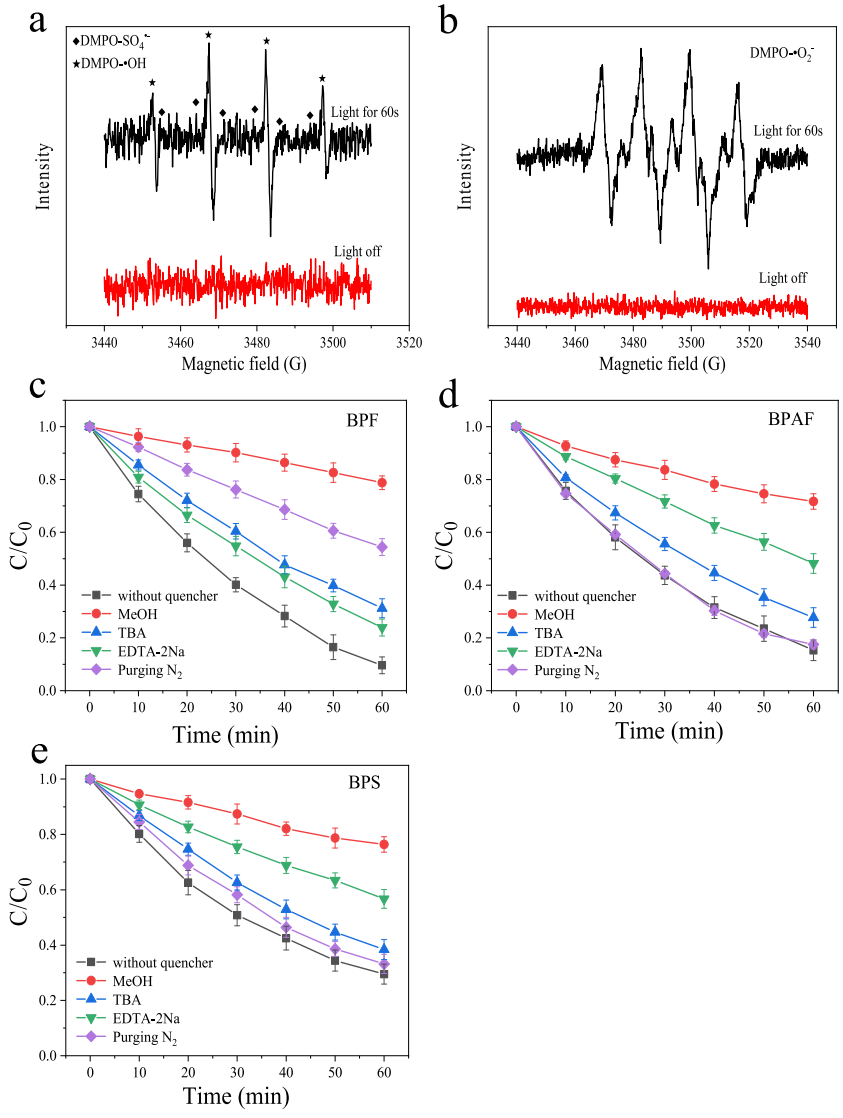

Fig. 7. ESR signals of the (a) DMPO-·OH and DMPO-$SO_4^{\bullet-}$, (b) DMPO-$^{\bullet}O_2^-$; and effects of various scavengers on the removal efficiency of (c) BPF, (d) BPAF, (e) BPS in the TiO_2NTAs/PMS/SL system. Reaction conditions: [PMS] = 0.5 mM, [MeOH] = [TBA] = 0.5 M, [EDTA-2Na] = 0.5 mM, [initial pH] = 7, T = 25 ℃.

appeared in all systems (data not shown), indicating that $^1O_2$ was not involved in three bisphenols degradation in this study.

Furthermore, to confirm the predominant reactive species working in the TiO_2NTAs/PMS/SL system, the quenching experiments were conducted. Generally, MeOH is employed to identify $SO_4^{\bullet-}$ and ·OH since it possesses high reaction constants with them ($1.2–2.8 \times 10^9$ M^{-1} s^{-1} for $SO_4^{\bullet-}$ and $1.6–7.7 \times 10^7$ M^{-1} s^{-1} for ·OH), while TBA is usually used to verify the presence of ·OH because it reacts with ·OH at a rate constant generally 3 orders of magnitude higher than that with $SO_4^{\bullet-}$ ($3.8–7.6 \times 10^8$ $M^{-1}s^{-1}$ for ·OH vs. $4.0–9.1 \times 10^5$ $M^{-1}s^{-1}$ for $SO_4^{\bullet-}$) (Wang et al., 2019). As presented in Fig. 7c-e, the degradation of three bisphenols was all intensively prevented (69.2% reduction for BPF, 56.4% reduction for BPAF and 46.9% reduction for BPS) after addition of 0.5 M MeOH (n[MeOH/PMS] = 1000), the residual oxidation of bisphenols might be attributed to the photocatalytic degradation of TiO_2NTAs and the PMS oxidation. However, when the same dose of TBA was added to the reaction system, the degradation efficiencies of three bisphenols were decreased by 21.6%, 12.4% and 8.9% for BPF, BPAF and BPS, respectively, which was much lower than that of MeOH. The above results manifested that both $SO_4^{\bullet-}$ and ·OH made contribution to the degradation of three bisphenols, and $SO_4^{\bullet-}$ played a more important role during this process. Besides, EDTA-2Na and purging N_2 were commonly employed to confirm the contribution of h^+ and $^{\bullet}O_2^-$, respectively. When purging N_2 was performed, the BPF degradation showed an obvious decrease (44.8% reduction), while negligible influence on BPAF and BPS degradation (2.2% reduction for BPAF and 3.7% reduction for BPS) was observed, suggesting that $^{\bullet}O_2^-$ was another dominant reactive species for BPF degradation, but not for BPAF and BPS. On the contrary, the degradation efficiencies of BPAF and BPS were remarkably prevented after the addition of EDTA-2Na as shown in Fig. 7d and e (32.9% reduction for BPAF and 27.2% reduction for BPS), suggesting that h^+ also played an important role in the degradation of both BPAF and BPS. Combining ESR measurements and quenching tests, it could be concluded that $SO_4^{\bullet-}$, ·OH, h^+, and $^{\bullet}O_2^-$ were all generated in the TiO_2NTAs/PMS/SL system. Among which, $SO_4^{\bullet-}$, ·OH and $^{\bullet}O_2^-$ were the main reactive species responsible for BPF degradation, while $SO_4^{\bullet-}$, ·OH and h^+ played the dominant role in BPAF and BPS degradation processes.

Obviously, the main difference in the reactive species that play a major role in the degradation of three bisphenols were $^{\bullet}O_2^-$ and h^+. This difference could be explained by that: the molecular structure of BPF had a high electron density and was easier to be oxidized, however, BPAF and BPS were relatively difficult to be degraded because of the electron-withdrawing F atom and SO_2 group, respectively. Based on previous reports, the oxidation capacity of $^{\bullet}O_2^-$ was much lower than that of h^+ (Hoffmann et al., 1995; Nosaka and Nosaka, 2017), thus, combined with the results of quenching experiments and ESR tests, it could be speculated that BPAF and BPS were difficult to be oxidized by $^{\bullet}O_2^-$, but could be easily oxidized by h^+. However, h^+ existed only on the surface of the catalyst, and had a much shorter lifetime (about 10 ns) than that of $^{\bullet}O_2^-$ (ms class) (Hoffmann et al., 1995; Nosaka and Nosaka, 2017; Liu et al., 2016), so the contaminants adsorbed only on the surface of the catalyst could be degraded by h^+. On the contrary, $^{\bullet}O_2^-$ could diffuse into solution and persist for a relatively long time, which greatly increased its exposure to pollutant (BPF). This also further explained why BPF had a higher degradation rate than that of BPAF and BPS in the same reaction system.

3.6.2. Identification of oxidation products

To fully understand the degradation processes of three bisphenols in the TiO_2NTAs/PMS/SL system, HPLC/ESI-QQQ were employed to identify the oxidation products of three bisphenols. The potential transformation products could be confirmed by comparing the total ion current (TIC) chromatograms of three bisphenols before and after degradation, the MS spectral of relevant intermediates and the corresponding fragment peaks were presented in Figs. 8–10.

For the degradation of BPF, a total of seven degradation intermediates (A1-A7) were detected. As shown in Fig. 8a, four peaks appeared at 31.65 min, 28.87 min, 8.42 min and 38.34 min with the m/z values of 215 Da (A1), 231 Da (A2), 247 Da (A3) and 279 Da (A4) were found, the corresponding mass spectra were shown in Fig. 8b-e. These peaks could be assigned to the hydroxylated BPAF since their m/z values were 16 Da, 32 Da, 48 Da and 80 Da larger than that of BPF ($m/z = 199$ Da), respectively. The peaks centered at 27.6 min and 38.3 min represented A5 ($m/z = 123$ Da) and A6 ($m/z = 137$ Da), respectively, which could be identified as the bond-cleavage products of BPF based on previous study (Yang et al., 2020). Besides, the peak at 7.7 min with $m/z = 397$ Da represent A7, which might be a coupling product since the m/z value was two times larger than that of BPF.

Five oxidation products (B1-B5) were identified during BPAF degradation. As presented in Fig. 9a, the peak at 34.2 min was composed of two products: B1 ($m/z = 351$ Da) and B2 ($m/z = 367$ Da), which could be classified as the hydroxylation products of BPAF because the m/z values of B1 and B2 were 16 Da and 32 Da greater than that of BPAF (335 Da), respectively. The compound B3 with peak time at 33.4 min was 383 Da, it was likely a product of carboxylation since it was 49 Da larger than that of BPAF. The peak centered at 36.2 min with 241 Da represented B4, it might come from the C–C bond cleavage involved in C═C, since the fragment losing a carbonyl group at $m/z = 212.9$ Da (Wang et al., 2019). Lastly, the peak at 33.6 min corresponded to the product B5 ($m/z = 223$ Da), which was 112 Da lower than that of BPAF. Since the molecular weight of benzene was 78 Da, thus it was likely that the loss of benzene occurred during the reaction process. Based on the previous study, B5 might be assigned to 4,4,4-trifluoro-3-hydroxy-3-(-trifluoromethyl)-kethoxal (Yang et al., 2019).

Four main intermediates were identified (C1-C4) during BPS degradation process. As depicted in Fig. 10a, the peak appeared at 6.02 min in the TIC chromatograms was composed of C1 ($m/z = 265$ Da) and C2 ($m/z = 297$ Da). They could be identified as the hydroxylation product of BPS since m/z values of C1 and C2 were 16 and 48 Da larger than that of BPS (249 Da). Besides, based on the ionization pattern, MS spectrum, and possible reaction pathway, the C3 ($m/z = 173$ Da) with the peak centered at 15.5 min might be assigned to 4-hydroxybenzenesulfonic acid, a product generated in the oxidation of the sulfur atom of BPS. Lastly, the m/z value of C4 centered around 30. 9 min was 357 Da, which could be identified as 2-(4-hydroxyphenoxy) bisphenol S according to previous study (Li et al., 2018).

3.6.3. Proposed degradation pathways and comparison

According to the identified oxidation products as discussed above, the degradation pathways of the three bisphenols in the TiO_2NTAs/PMS/SL system were proposed. As shown in Fig. 11a, there were three possible degradation pathways occurred in the BPF degradation process: (i)·OH attacked the benzene ring (electron-rich group) of BPF, resulting in the formation of hydroxylation product A1. Then, A1 was further attacked by ·OH and transformed into A2 and A3. Thereafter, the ring-cleavage reactions would take place under the continuous hydroxylation of benzene ring, leading to the formation of A4; (ii) the reactive species generated in the system might directly attack BPF and produce the bond-cleavage products: A5 and A6. These two products might be further converted to ring-cleavage products under the continuous oxidation of the reactive species; (iii) the phenoxy radical might be formed during chemical oxidation of phenols, where the single electron transfer process would happen and form radicals. These radicals would couple with each other at different positions and then generate dimers. Based on the possible degradation pathway, in this study, the phenoxy radical AR might be formed during the oxidation of BPF, and then produce A7 by self-coupling. The similar phenomenon was also reported by Yang et al. Yang et al. (2020), who speculated that the radical AR was formed during the oxidation of BPF by ferrate.

For BPAF and BPS, single electron transfer process might also occur during their degradation processes. Namely, the reactive species

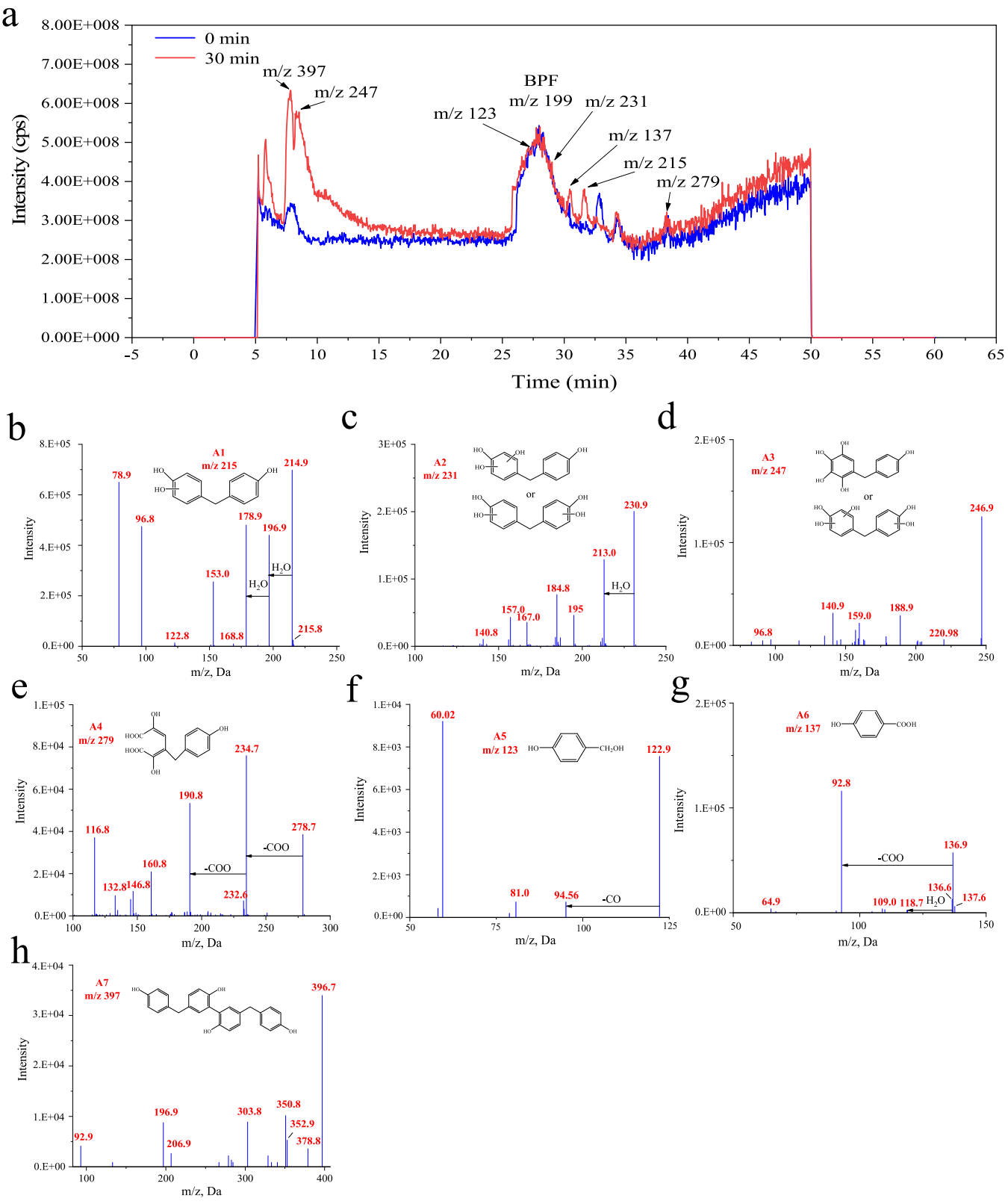

Fig. 8. HPLC/ESI-QQQ TIC chromatograms of the BPF samples at different reaction time (a), and the extracted molecular ion mass spectra of the relevant oxidation products (b), (c), (d), (e), (f), (g), (h). Reaction conditions: [PMS] = 0.5 mM, [BPF] = 10 mg/L, [initial pH] = 7, T = 25 °C.

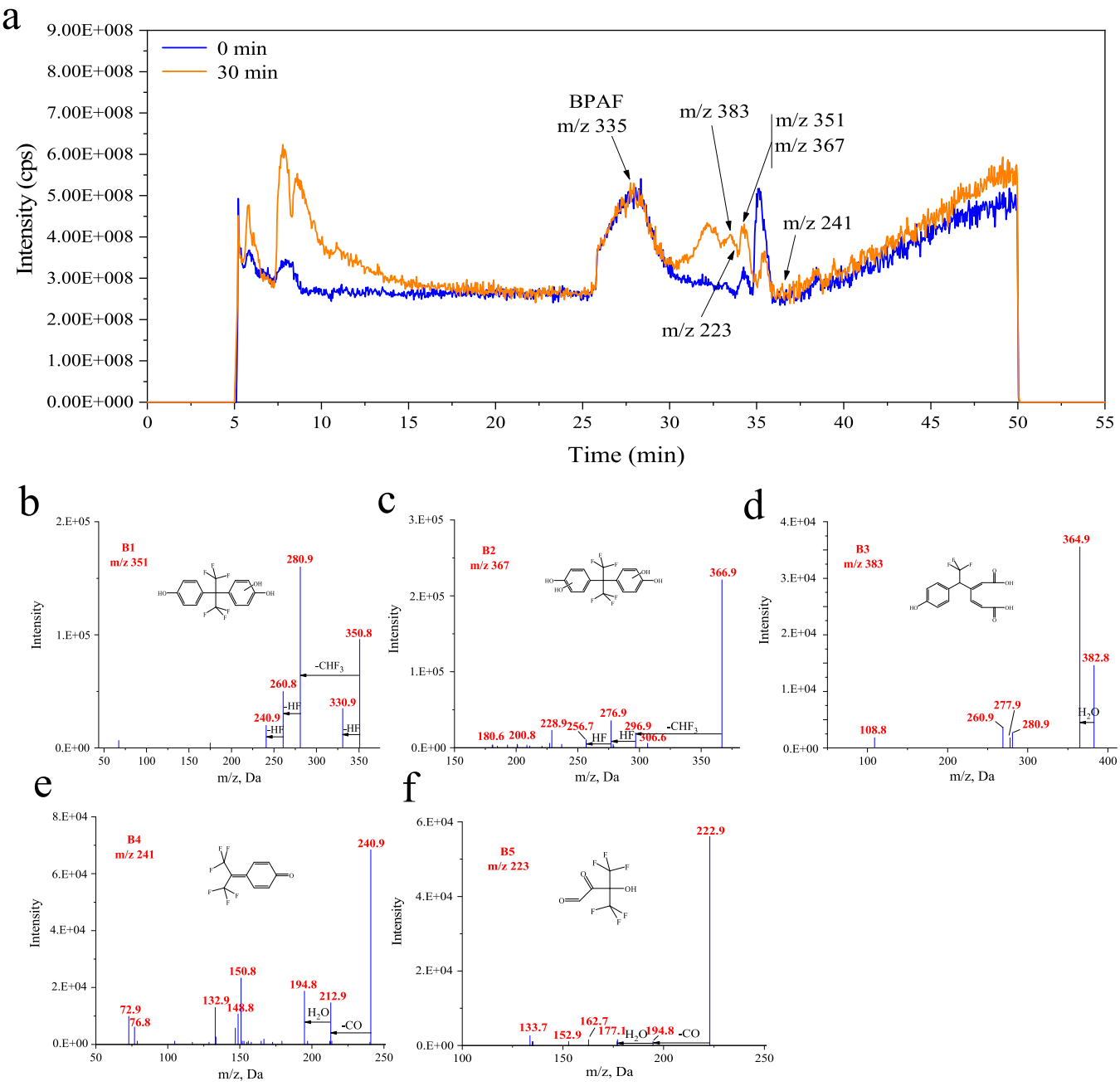

Fig. 9. HPLC/ESI-QQQ TIC chromatograms of the BPAF samples at different reaction time (a), and the extracted molecular ion mass spectra of the relevant oxidation products (b), (c), (d), (e), (f). Reaction conditions: [PMS] = 0.5 mM, [BPAF] = 10 mg/L, [initial pH] = 7, T = 25 °C.

generated in the system would attack the electron rich moiety (phenol moiety) of BPS/BPAF first and acquire one electron. Because of the delocalization of the lone pair electron, BPAF and BPS might transform into phenoxy radicals (BR1 and CR1) and other resonance forms (BR2, BR3, CR2, CR3). Then, the degradation pathways were separated to two sections. Firstly, the reactive species would attack BR2 and CR2 with the high electron density at *ortho*-position through oxygen transfer process, and followed by formation of the hydroxylation products (B1, B2 in BPAF, and C1, C2 in BPS). In the hydroxylation of BPAF, B3 would be generated by splitting benzene ring since the hydroxyl group was embedded in the *ortho*-position of benzene ring (Wang et al., 2019). Besides, the self-coupling would take place on CR2 via carbon-oxygen (C-O) or carbon-carbon (C-C), resulting in the formation of dimers C4. Secondly, due to the high electron density of the *para*-position, a β-scission would occur in BR3 and CR3, resulting in the formation of cations (BR4 and CR4) and radicals (BR5 and CR5). Next, these compounds would convert to C-C bond cleavage products (B4 and hydroquinone in BPAF) and S-C bond cleavage products (C3 and hydroquinone in BPS). It should be noted that the chemical structure of di-hydroxy (*ortho*-position) products and hydroquinone was unstable and would transform into hydrogen-atom-transfer and ring-cleavage products (Han et al., 2015; Xie et al., 2016). The ring-cleavage products might be further oxidized into lower molecular weight products (B5).

Based on the above analysis, it was found that the bond-cleavage reaction and hydroxylation reaction occurred in all three bisphenols degradation processes. In addition, the benzene ring splitting happened only in BPAF degradation, while the self-coupling reaction occurred

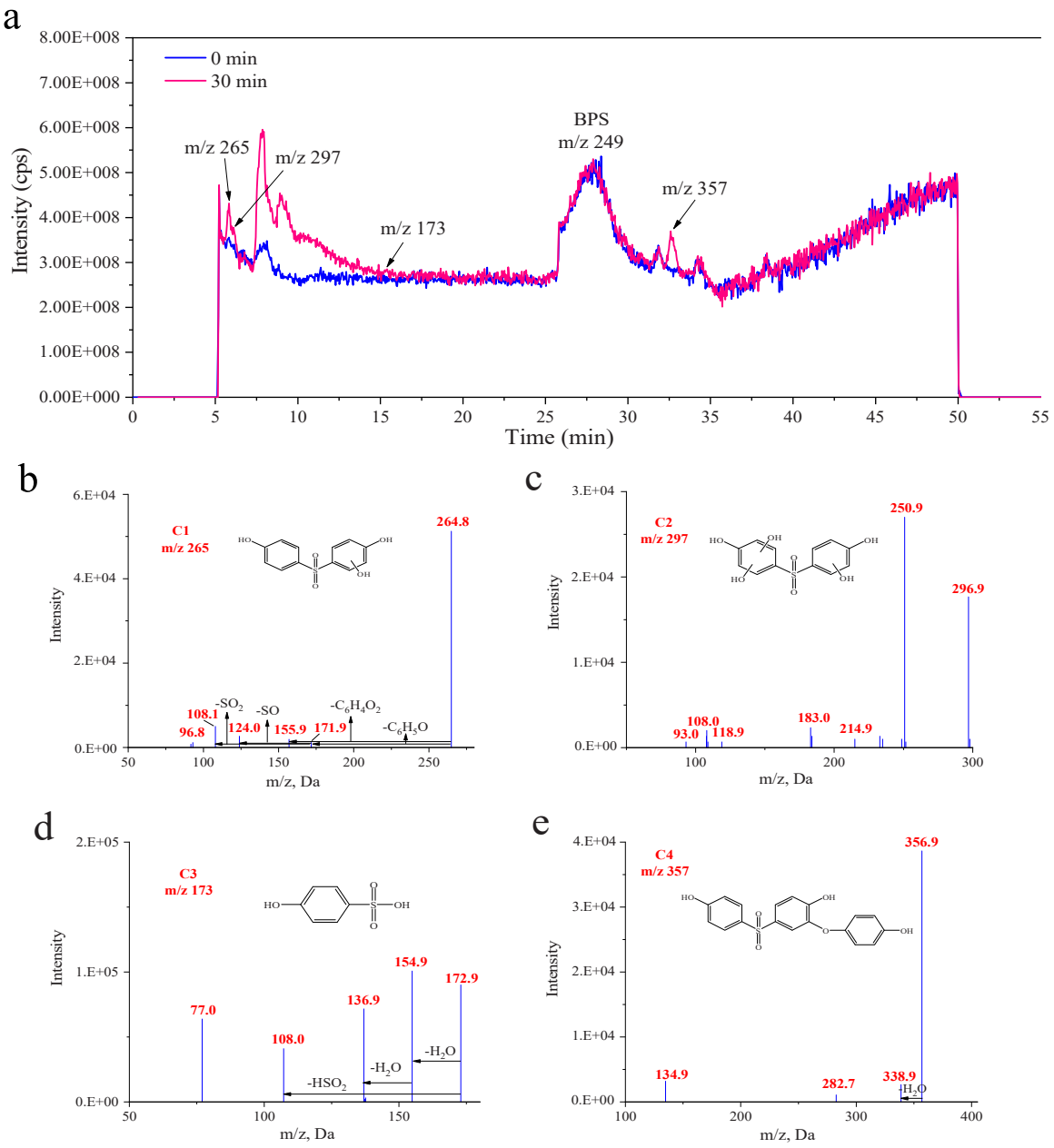

Fig. 10. HPLC/ESI-QQQ TIC chromatograms of the BPS samples at different reaction time (a), and the extracted molecular ion mass spectra of the relevant oxidation products (b), (c), (d), (e). Reaction conditions: [PMS] = 0.5 mM, [BPS] = 10 mg/L, [initial pH] = 7, T = 25 °C.

only in BPF and BPS degradation processes. In comparison, no self-coupling product was found in the BPAF degradation process, implying that BPAF was stepwise oxidized in the TiO_2NTAs/PMS/SL system.

4. Conclusions

In this work, TiO_2 photocatalytic activation of PMS under simulated sunlight irradiation for removal of three bisphenols (BPF, BPAF and BPS) was investigated, and the degradation behaviors of three bisphenols were systematically studied and compared.

(1) The degradation of three bisphenols in the TiO_2NTAs/PMS/SL system followed the first-order rate law, and the acidic conditions were more favorable for three bisphenols degradation. In a wide pH range, BPF was more easily oxidized than BPAF and BPS.

(2) HCO_3^- showed an inhibitory effect on three bisphenols degradation, and the inhibition enhanced with the dose increased. Cl^- and HA have a dual-effect on three bisphenols degradation. With the concentration of Cl^- increased, the removal efficiency decreased first and then increased, while, HA exhibited a completely opposite trend compared to Cl^-.

(3) The $SO_4^{\bullet-}$, ·OH, h^+, and $^{\bullet}O_2^-$ were all involved in three bisphenols degradation. Among which, $SO_4^{\bullet-}$, ·OH and $^{\bullet}O_2^-$ were the dominant reactive species responsible for BPF degradation, while the degradation of BPAF and BPS were primarily performed by $SO_4^{\bullet-}$, ·OH and h^+.

(4) The degradation pathways of three bisphenols were proposed. Besides some common degradation pathways, including hydroxylation of the benzene ring and bond-cleavage, there were some specific pathways such as the benzene ring splitting

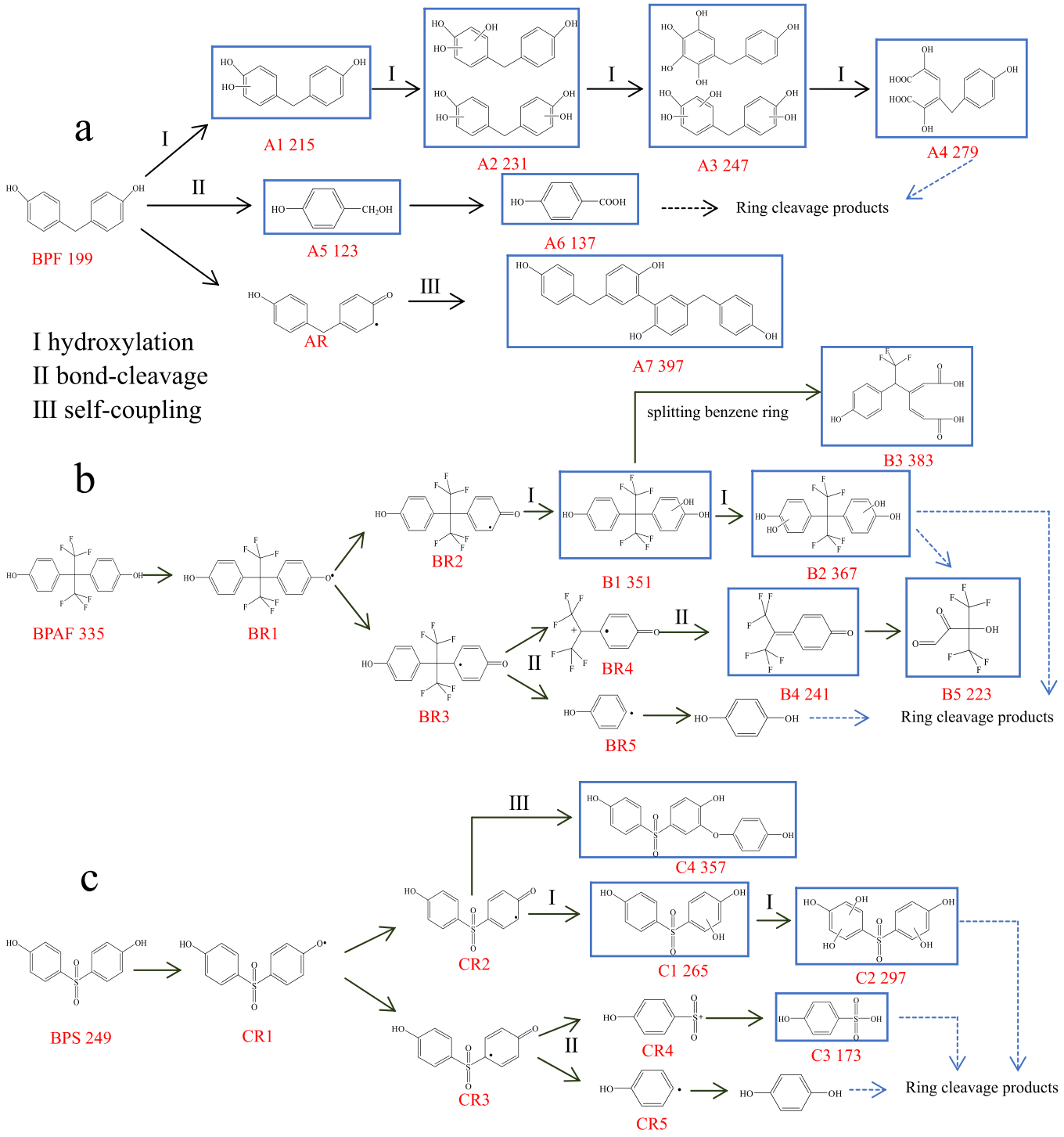

Fig. 11. Proposed degradation pathways of (a) BPF, (b) BPAF and (c) BPS in TiO_2NTAs/PMS/SL system.

happened in BPAF degradation process, and the self-coupling reaction occurred in BPF and BPS oxidation processes.

This work is hope to provide useful references for analyzing the transformation of the three bisphenols in different reactive species predominant oxidation systems, and selecting the suitable advanced oxidation systems to effectively degrade the specific bisphenols in practical application.

CRediT authorship contribution statement

Jialin Jia: Conceptualization, Investigation, Data Curation, Formal analysis, Validation, Writing – original draft, Writing – review & editing. **Dongmei Liu, Jiayu Tian**: Writing – review & editing, Funding acquisition, Resources. **Qiao Wang, Huarui Li, Jiaxin Ni**: Data curation, Methodology. **Fuyi Cui**: Investigation, Data curation.

Declaration of Competing Interest

The authors declare that they have no known competing financial

interests or personal relationships that could have appeared to influence the work reported in this paper.

Acknowledgments

This work was supported by the funds of the State Key Laboratory of Urban Water Resource and Environment (HIT, 2021TS03), National Natural Science Foundation of China (NO. 51978232), Open Project of State Key Laboratory of Urban Water Resource and Environment, Harbin Institute of Technology (No. HC202154), Natural Science Foundation of Hebei Province (No. E2019202012), Natural Science Foundation of Tianjin (No. E2019080401), and the Science and Technology Research Program for Colleges and Universities in Hebei Province (No. QN2019022).

Appendix A. Supporting information

Supplementary data associated with this article can be found in the online version at doi:10.1016/j.jhazmat.2021.127434.

References

Akpan, U.G., Hameed, B.H., 2009. Parameters affecting the photocatalytic degradation of dyes using TiO_2-based photocatalysts: a review. J. Hazard. Mater. 170, 520–529.
Andersson, M., Osterlund, L., Ljungstrom, S., Palmqvist, A., 2002. Preparation of nanosize anatase and rutile TiO_2 by hydrothermal treatment of microemulsions and their activity for photocatalytic wet oxidation of phenol. J. Phys. Chem. B 106, 10674–10679.
Anipsitakis, G.P., Dionysiou, D.D., 2004. Transition metal/UV-based advanced oxidation technologies for water decontamination. Appl. Catal. B Environ. 54, 155–163.
Ao, X., Liu, W., 2017. Degradation of sulfamethoxazole by medium pressure UV and oxidants: peroxymonosulfate, persulfate, and hydrogen peroxide. Chem. Eng. J. 313, 629–637.
Chen, W., Huang, C., 2015. Mineralization of aniline in aqueous solution by electrochemical activation of persulfate. Chemosphere 125, 175–181.
Chen, X., Oh, W., Lim, T., 2018. Graphene-and CNTs-based carbocatalysts in persulfates activation: material design and catalytic mechanisms. Chem. Eng. J. 354, 941–976.
Chen, X.Y., Wang, W.Ping, H. X, Hong, C.L., Zhu, F.X., Yao, Y.L., Xue, Z.Y., 2012. Accelerated TiO_2 photocatalytic degradation of Acid Orange 7 under visible light mediated by peroxymonosulfate. Chem. Eng. J. 193–194, 290–295.
Cho, Y.M., Choi, W.Y., 2002. Visible light-induced reactions of humic acids on TiO_2. J. Photochem. Photobiol. A 148, 129–135.
Cui, Y.J., Ding, Z.X., Liu, P., Antonietti, M., Fu, X.Z., Wang, X.C., 2012. Metal-free activation of H_2O_2 by g-C_3N_4 under visible light irradiation for the degradation of organic pollutants. Phys. Chem. Chem. Phys. 14, 1455–1462.
Deceuninck, Y., Bichon, E., Marchand, P., Boquien, C.-Y., Legrand, A., Boscher, C., Antignac, J.P., Le, B., 2015. Bizec, Determination of bisphenol A and related substitutes/analogues in human breast milk using gas chromatography-tandem mass spectrometry. Anal. Bioanal. Chem. 407, 2485–2497.
Duan, X.G., Su, C., Zhou, L., Sun, H.Q., Suvorova, A., Odedairo, T., Zhu, Z.H., Shao, Z.P., Wang, S.B., 2016. Surface controlled generation of reactive radicals from persulfate by carbocatalysis on nanodiamonds. Appl. Catal. B Environ. 194, 7–15.
Elias, H., Gotz, U., Wannowius, K.J., 1994. Kinetics and mechanism of the oxidation of sulfur(Iv) by peroxomonosulfuric acid anion. Atmos. Environ. 28, 439–448.
Fic, A., Bojana, E., Sollner, D., Filipi, M., Peterlin, M., 2013. Mutagenicity and DNA damage of bisphenol A and its structural analogues in HepG2 cells. Arch. Ind. Hyg. Toxicol. 64, 189–200.
Gao, Y., Jiang, J., Zhou, Y., Pang, S.Y., Ma, J., Jiang, C.C., Yang, Y., Huang, Z.S., Gu, J., Guo, Q., Duan, J.B., Li, J., 2018. Chlorination of bisphenol S: kinetics, products, and effect of humic acid. Water Res. 131, 208–217.
Gao, Y.W., Li, S.M., Li, Y.X., Yao, L.Y., Zhang, H., 2017. Accelerated photocatalytic degradation of organic pollutant over metal-organic framework MIL-53(Fe) under visible LED light mediated by persulfate. Appl. Catal. B Environ. 202, 165–174.
Ghauch, A., Tuqan, A.M., 2012. Oxidation of bisoprolol in heated persulfate/H_2O systems: kinetics and products. Chem. Eng. J. 183, 162–171.
Halmann, M.M., 1996. Photodegradation of Water Pollutants. CRC Press, New York, USA.
Han, Q., Wang, H.J., Dong, W.Y., Liu, T.Z., Yin, Y.L., Fan, H.K., 2015. Degradation of bisphenol A by ferrate(VI) oxidation: kinetics, products and toxicity assessment. Chem. Eng. J. 262, 34–40.
Hashimoto, Y., Nakamura, M., 2000. Estrogenic activity of dental materials and bisphenol-A related chemicals in vitro. Dent. Mater. J. 19, 245–262.
Hoffmann, M.R., Martin, S.T., Choi, W.Y., Bahnemann, D.W., 1995. Environmental applications of semiconductor photocatalysis. Chem. Rev. 95, 69–96.
Hu, J., Dong, H., Qu, J., Qiang, Z., 2017. Enhanced degradation of iopamidol by peroxymonosulfate catalyzed by two pipe corrosion products (CuO and δ-MnO_2). Water Res. 112, 1–8.
Jia, J.J., Liu, D.M., Tian, J.Y., Wang, W., Ni, J.X., Wang, X., 2020. Visible-light-excited humic acid for peroxymonosulfate activation to degrade bisphenol A. Chem. Eng. J. 400, 125853.
Jia, J.L., Liu, D.M., Wang, S.X., Li, H.R., Ni, J.X., Li, X.B., Tian, J.Y., Wang, Q., 2020. Visible-light-induced activation of peroxymonosulfate by TiO_2 nano-tubes arrays for enhanced degradation of bisphenol A. Sep. Purif. Technol. 253, 117510.
Jiang, J., Pang, S.Y., Ma, J., 2010. Role of ligands in permanganate oxidation of organics. Environ. Sci. Technol. 44, 4270–4275.
Khan, S., Han, C., Khan, H.M., Boccelli, D.L., Nadagouda, M.N., Dionysiou, D.D., 2017. Efficient degradation of lindane by visible and simulated solar light-assisted S-TiO_2/peroxymonosulfate process: kinetics and mechanistic investigations. Mol. Catal. 428, 9–16.
Kuehn, D.W., Snyder, R.W., Davis, A., Painter, P.C., 1982. Characterization of vitrinite concentrates. 1. Fourier Transform infrared studies. Fuel 61, 682–694.
Li, D., Jia, J.L., Zheng, T., Cheng, X.W., Yu, X.J., 2016. Construction and characterization of visible light active Pd nano-crystallite decorated and C–N–S-co-doped TiO_2 nanosheet array photoelectrode for enhanced photocatalytic degradation of acetylsalicylic acid. Appl. Catal. B Environ. 188, 259–271.
Li, D., Zhang, X.Y., Zhang, W., 2021. Designing a new reaction system by stacking use of Ti mesh supported Ag/NTiO_2 nano-sheets for enhanced photocatalytic degradation of bisphenol A. Chem. Eng. J. 405, 126867.
Li, H.R., Tian, J.Y., Zhu, Z.G., Cui, F.Y., Zhu, Y.A., Duan, X.G., Wang, S.B., 2018. Magnetic nitrogen-doped nanocarbons for enhanced metal-free catalytic oxidation: integrated experimental and theoretical investigations for mechanism and application. Chem. Eng. J. 354, 507–516.
Li, J., Yan, P.S., Zhou, Y., Sun, S.F., Wang, L.H., Wang, Z., Gao, Y., Yang, Y., Jiang, J., 2018. Transformation of bisphenol AF and bisphenol S by manganese dioxide and effect of iodide. Water Res. 143, 47–55.
Liao, C., Liu, F., Moon, H., Yamashita, N., Yun, S., Kannan, K., 2012. Bisphenol analogues in sediments from industrialized areas in the United States, Japan, and Korea: spatial and temporal distributions. Environ. Sci. Technol. 46, 11558–11565.
Liu, C., Kong, D.S., Hsu, P.C., Yuan, H.T., Lee, H.W., Liu, Y.Y., Wang, H.T., Wang, S., Yan, K., Lin, D.C., Maraccini, P.A., Parker, K.M., Boehm, A.B., Cui, Y., 2016. Rapid water disinfection using vertically aligned MoS_2 nanofilms and visible light. Nat. Nanotechnol. 11, 1098–1104.
Liu, J., Zhou, J., Ding, Z., Zhao, Z., Xu, X., Fang, Z., 2017. Ultrasound irritation enhanced heterogeneous activation of peroxymonosulfate with Fe_3O_4 for degradation of azo dye. Ultrason. Sonochem. 34, 953–959.
Moreman, J., Lee, O., Trznadel, M., David, A., Kudoh, T., Tyler, C., 2017. Acute toxicity, teratogenic and estrogenic effects of Bisphenol A and its alternative replacements Bisphenol S, Bisphenol F and Bisphenol AF in zebrafish embryo-larvae. Environ. Sci. Technol. 51, 12796–12805.
Newbold, R.R., Jefferson, W.N., Padilla-Banks, E., 2009. Prenatal exposure to bisphenol a at environmentally relevant doses adversely affects the murine female reproductive tract later in life. Environ. Health Perspect. 117, 879–885.
Nie, M., Yan, C., Li, M., Wang, X., Bi, W., Dong, W., 2015. Degradation of chloramphenicol by persulfate activated by Fe^{2+} and zerovalent iron. Chem. Eng. J. 279, 507–515.
Nosaka, Y., Nosaka, A.Y., 2017. Generation and Detection of Reactive Oxygen Species in Photocatalysis. Chem. Rev. 117, 11302–11336.
Oh, W., Lok, L., Veksha, A., Giannis, A., Lim, T., 2018. Enhanced photocatalytic degradation of bisphenol A with Ag-decorated S-doped g-C_3N_4 under solar irradiation: performance and mechanistic studies. Chem. Eng. J. 333, 739–749.
Oh, W.D., Dong, Z., Lim, T.T., 2016. Generation of sulfate radical through heterogeneous catalysis for organic contaminants removal: current development, challenges and prospects. Appl. Catal. B Environ. 194, 169–201.
Qi, C., Liu, X., Ma, J., Lin, C., Li, X., Zhang, H., 2016. Activation of peroxymonosulfate by base: implications for the degradation of organic pollutants. Chemosphere 151, 280–288.
Richter, C.A., Birnbaum, L.S., Farabollini, F., Newbold, R.R., Rubin, B.S., Talsness, C.E., Vandenbergh, J.G., Walser-Kuntz, D.R., vom Saal, F.S., 2007. In vivo effects of bisphenol A in laboratory rodent studies. Reprod. Toxicol. 24, 199–224.
Rochester, J.R., Bolden, A.L., 2015. Bisphenol S and F: a systematic review and comparison of the hormonal activity of bisphenol A substitutes. Environ. Health Perspect. 123, 643–650.
Shi, W.D., Yan, Y., Xu, Y., 2013. Microwave-assisted synthesis of nano-scale $BiVO_4$ photocatalysts and their excellent visible-light-driven photocatalytic activity for the degradation of ciprofloxacin. Chem. Eng. J. 215–216, 740–746.
Song, S.J., Ruan, T., Wang, T., Liu, R.Z., Jiang, G.B., 2012. Distribution and preliminary exposure assessment of bisphenol AF (BPAF) in various environmental matrices around a manufacturing plant in China. Environ. Sci. Technol. 46, 13136–13143.
Stone, A.T., 1987. Reductive dissolution of manganese(III/Iv) oxides by substituted phenols. Environ. Sci. Technol. 21, 979–988.
Tan, C., Gao, N., Deng, Y., Li, L., Deng, J., Zhou, S., 2015. Kinetic oxidation of antipyrine in heat-activated persulfate. Desalin. Water Treat. 53, 263–271.
Vassallo, A.M., Lockhart, N.C., Hanna, J.V., Chamberlein, R., Painter, P.C., Sobkowiak, M., 1991. Infrared and nuclear magnetic resonance spectroscopy of density fractions from Callide coal. Energy Fuels 5, 477–482.
Wacławek, S., Lutze, H.V., Grübel, K., Padil, V.V.T., Černík, M., Dionysiou, D.D., 2017. Chemistry of persulfates in water and wastewater treatment: a review. Chem. Eng. J. 330, 44–62.
Wang, Q., Liu, Z.Q., Liu, D.M., Liu, G.S., Yang, M., Cui, F.Y., Wang, W., 2018. Ultrathin two-dimensional BiOBrxI1-x solid solution with rich oxygen vacancies for enhanced visible-light-driven photoactivity in environmental remediation. Appl. Catal. B Environ. 236, 222–232.

Wang, Q., Cao, Y., Zeng, H., Liang, Y.H., Ma, J., Lu, X.H., 2019. Ultrasound-enhanced zero-valent copper activation of persulfate for the degradation of bisphenol AF. Chem. Eng. J. 378, 122143.

Wang, S.X., Tian, J.Y., Wang, Q., Xiao, F., Gao, S.S., Shi, W.X., Cui, F.Y., 2019. Development of CuO coated ceramic hollow fiber membrane for peroxymonosulfate activation: a highly efficient singlet oxygen-dominated oxidation process for bisphenol a degradation. Appl. Catal. B Environ. 256, 117783.

Wang, Y., Sun, H., Ang, H.M., Tadé, M.O., Wang, S., 2015. 3D-hierarchically structured MnO_2 for catalytic oxidation of phenol solutions by activation of peroxymonosulfate: structure dependence and mechanism. Appl. Catal. B Environ. 164, 159–167.

Wang, Z.H., Yuan, R.X., Guo, Y.G., Xu, L., Liu, J.S., 2011. Effects of chloride ions on bleaching of azo dyes by Co^{2+}/oxone reagent: kinetic analysis. J. Hazard Mater. 190, 1083–1087.

Xie, J.H., Ma, L., Lam, W.W.Y., Lau, K.C., Lau, T.C., 2016. Hydrogen atom transfer reactions of ferrate(vi) with phenols and hydroquinone. Correlation of rate constants with bond strengths and application of the Marcus cross relation. Dalton Trans. 45, 70–73.

Xu, B.T., Ahmed, M.B., Zhou, J.L., Altaee, A., 2020. Visible and UV photocatalysis of aqueous perfluorooctanoic acid by TiO_2 and peroxymonosulfate: Process kinetics and mechanistic insights. Chemosphere 243, 125366.

Yamazaki, E., Yamashita, N., Taniyasu, S., Lam, J., Lam, P.K.S., Moon, H.-B., Jeong, Y., Kannan, P., Achyuthan, H., Munuswamy, N., Kannan, K., 2015. Bisphenol A and other bisphenol analogues including BPS and BPF in surface water samples from Japan, China, Korea and India. Ecotoxicol. Environ. Saf. 122, 565–572.

Yang, T., Wang, L., Liu, Y.L., Huang, Z.S., He, H.Y., Wang, X.S., Jiang, J., Gao, D.W., Ma, J., 2019. Comparative study on ferrate oxidation of BPS and BPAF: kinetics, reaction mechanism, and the improvement on their biodegradability. Water Res. 148, 115–125.

Yang, T., Wang, L., Liu, Y.L., Zhang, W., Cheng, H.J., Liu, M.C., Ma, J., 2020. Ferrate oxidation of bisphenol F and removal of oxidation products with ferrate resulted particles. Chem. Eng. J. 383, 123167.

Yuan, R., Ramjaun, S.N., Wang, Z., Liu, J., 2011. Effects of chloride ion on degradation of Acid Orange 7 by sulfate radical-based advanced oxidation process: implications for formation of chlorinated aromatic compounds. J. Hazard Mater. 196, 173–179.

Zhang, H., Zhao, L.X., Geng, F.L., Guo, L.H., Wan, B., Yang, Y., 2016. Carbon dots decorated graphitic carbon nitride as an efficient metal-free photocatalyst for phenol degradation. Appl. Catal. B Environ. 180, 656–662.

Zhang, T.H., Liu, Y.J., Rao, Y.D., Li, X.P., Yuan, D.L., Teng, S.F., Zhao, Q.X., 2020. Enhanced photocatalytic activity of TiO_2 with acetylene black and persulfate for degradation of tetracycline hydrochloride under visible light. Chem. Eng. J. 384, 123350.

Zhang, W., Zhou, L., Deng, H.P., 2016. Ag modified g-C_3N_4 composites with enhanced visible-light photocatalytic activity for diclofenac degradation. J. Mol. Catal. A Chem. 423, 270–276.

Zhou, J., Xiao, J.H., Xiao, D.X., Guo, Y.G., Fang, C.L., Lou, X.Y., Wang, Z.H., Liu, J.S., 2015. Transformations of chloro and nitro groups during the peroxymonosulfate-based oxidation of 4-chloro-2-nitrophenol. Chemosphere 134, 446–451.

Zhu, M., Chen, X.Y., Li, Y.Y., Yin, N.Y., Faiola, F., Qin, Z.F., Wei, W.J., 2018. Bisphenol F disrupts thyroid hormone signaling and postembryonic development in Xenopus laevis. Environ. Sci. Technol. 52, 1602–1611.